THE JOURNAL OF PHYSICAL CHEMISTRY B

ARTICLE

pubs.acs.org/JPCB

Evidence of Multiple Folding Pathways for the Villin Headpiece Subdomain

Li Zhu,[†,‡] Kingshuk Ghosh,[§] Michael King,[†] Troy Cellmer,[∥] Olgica Bakajin,[⊥] and Lisa J. Lapidus*[,†]

[†]Department of Physics and Astronomy, Michigan State University, East Lansing, Michigan 48824, United States

[‡]Advanced Photonics Center, Southeast University, Nanjing 210096, China

[§]Department of Physics and Astronomy, University of Denver, Denver, Colorado 80208, United States

[∥]Laboratory of Chemical Physics, Building 5, National Institute of Diabetes and Digestive and Kidney Diseases, National Institutes of Health, Bethesda, Maryland 20892, United States

[⊥]Center for Biophotonics Science and Technology, University of California, Davis, Sacramento, California, United States

ABSTRACT: The defining property of two-state models of protein folding is that the measured relaxation rates are independent of the starting conditions and only depend on the final conditions. In this work we compare the kinetics of the very fast folding villin subdomain measured after a large change in denaturant concentration using an ultrarapid microfluidic mixer with the kinetics measured after a small temperature change in a laser T-jump experiment and find a significant difference in the observed folding kinetics. The final conditions of temperature and denaturant concentration and the use of tryptophan fluorescence as a probe are the same in both experiments, while the initial conditions are very different. The slower mixing kinetics show no evidence of the faster phase in T-jump experiments, which would support models of on- or off-pathway intermediates. Rather we interpret the combined mixer and T-jump experiments as evidence of an ensemble of unfolded states, some of which are traps. The ensemble after dilution from high denaturant is more expanded than the ensemble after an increase in temperature and, on average, takes longer to reach the native state.

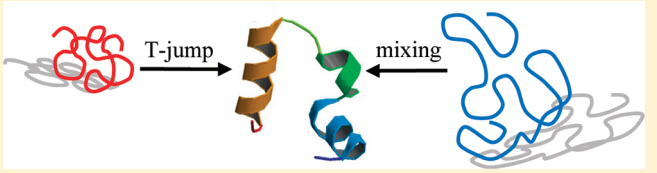

INTRODUCTION

A hallmark of simple two-state protein folding models is that the folding or unfolding rate is independent of the initial conditions of the experiment. Instead, the rate is determined by the free energy barrier after the change in solvent conditions that starts the experiment and a pre-exponential term that is constant under all conditions. Such models predict that the observed relaxation rate will be the same as solvent conditions are changed to the same final conditions (i.e., the denaturant is diluted or temperature is raised). Indeed, experimental chevron plots of relaxation rates vs denaturant concentration usually show good overlap in observed rates from folding experiments started from high denaturant and unfolded experiments started from no denaturant,[1,2] and such measurements have made simple models one of the leading interpretations of protein folding for many years.

On the other hand, energy landscape theory of protein folding suggests that, because proteins fold efficiently and quickly, progress toward the folded structure of a protein is "minimally frustrated" and is associated with a continuous decrease in energy to produce a "folding funnel".[3,4] Such a view logically raises the possibility of multiple parallel pathways down this funnel, but there has been scant experimental evidence for this phenomenon, even for the fastest folders with minimal free energy barriers between the folded and unfolded states. For example, the fastest folding mutants of lambda repressor show probe dependent kinetics, which in one case was interpreted as diffusion on a multidimensional landscape[5] but in another case was interpreted with a 1-dimensional landscape with no barrier (a downhill folder) with each probe having a different sensitivity to the folding reaction coordinate.[6] As was pointed out by Hagen, probe-dependent kinetics does not exclusively signify downhill folding if there is more than one reaction coordinate to the landscape.[7]

In this work we observe relaxation on the energy landscape from two different types of perturbations, temperature and denaturant. The subject of this study is the 35 residue subdomain of the villin headpiece (HP-35). This protein, one of the fastest folding proteins yet found, has been extensively studied by molecular dynamics simulations.[8−19] It has also been studied in laser T-jump experiments by measuring tryptophan (Trp) fluorescence intensity[20,21] and infrared absorption.[22] A single fast relaxation ($\sim 4\,\mu s$) is observed after a temperature increase of ~ 10 C that can be well modeled by a 1-d free energy surface with a small barrier between folded and unfolded states.[23] Here we find the kinetics significantly slower for the same final conditions when folding is initiated by ultrarapid dilution of denaturant at a constant temperature. Since the sequence and folding probe is identical in these experiments, we conclude that the unfolded ensemble after dilution of denaturant is conformationally distinct from the ensemble after increase in temperature.

Received: July 1, 2011
Revised: September 14, 2011
Published: September 16, 2011

EXPERIMENTAL METHODS

HP-35 was produced by solid phase synthesis by AnaSpec (San Jose, CA) and purified to >98%. The sequence is Ac-LSDED FKAVF GMTRS AFANL PLWKQ QHLKK EKGLF-NH_2 (note that this sequence is slightly different than that used in refs 20 and 21 in that the N- and C-termini are acetylated and amidated (i.e., "capped"), respectively, thereby eliminating a positive charge and a negative charge). For mixing experiments, the protein was dissolved in 20 mM acetate buffer at pH 4.9 and 6 M GdnHCl at final protein concentration of 300 μM as measured from the Trp UV absorption peak. The mixing buffer was 20 mM sodium acetate buffer at pH 4.8 with the final concentration of GdnHCl.

Folding experiments were conducted using a microfluidic ultrarapid mixer of the type developed by Knight et al[24] and Hertzog et al[25,26] and modified by Yao et al.[27] The mixer is constructed from a 500 μm thick fused silica wafer with channels typically etched 10 μm deep and a second 170 μm wafer bonded on top to seal the device. All flows are in the laminar regime and the concentration profile can be computed from the applied pressures by mathematical simulations using a finite element scheme (COMSOL Multiphysics, Stockholm, Sweden). The flow and concentration fields in these mixers are governed by the steady-state incompressible Navier–Stokes equation and the convective-diffusion equation for the faster diffusing reactant with lower Peclet number.

$$\rho(\vec{V}\cdot\nabla)\vec{V} = -\nabla P + \mu\nabla^2\vec{V} \quad (1)$$

$$\nabla\cdot\vec{V} = 0 \quad (2)$$

$$\vec{V}\cdot\nabla C = D\nabla^2 C \quad (3)$$

where $\vec{V}$ is the flow velocity, P is the pressure, ρ is the fluid density, and μ is the dynamic viscosity which is dependent on solvent composition and temperature. D and C are the diffusivity and the concentration of the reactant, respectively. For direct comparison with the experimental measurements of tryptophan fluorescence quenching by KI, we applied the appropriate fluid properties of aqueous solutions of KI in the control volume. Previous work has shown that these mixers are well characterized, are understood quantitatively, and can be accurately modeled.[25−27]

Determining the mixing time has been a somewhat controversial subject in the field. It is important to recognize the difference between "mixing time" and "dead time." The mixing time is the time to uniformly change the concentration of any relevant solute in the system. It is usually measured using an extremely fast reaction (i.e., diffusion-limited) and can be quantitatively defined in a number of ways. In contrast, the dead time is the time during which no measurement can be made even if mixing is complete. It is usually measured using a slower bimolecular reaction and multiple measurements of different concentrations are used to determine the first measurable time point after mixing. This is relevant to turbulent mixers in which turbulence prevents optical measurements until it has subsided. Laminar flow mixers permit measurements during the mixing process and calculation of laminar streamlines can accurately determine time after mixing. Thus there is no dead time in this mixer, and we only measure the mixing time in this work.

Figure 1b shows the comparison of measured and simulated concentration vs time after mixing, showing good agreement. The simulation is used to convert position to time after initiation of mixing using the position dependent velocity from the numerical model. Flow rates in the exit channel after the mixing region are also analytically calculated from a resistance model of the chip using measured values of viscosity for a given denaturant concentration and temperature and checked experimentally using particle image velocimetry.[26] Clogging of chips is an occasional problem for any microfluidic device but does not pose a systematic uncertainty on the velocity. If one of the side channels, which each contribute almost half the total flow, is clogged, the narrow jet of protein is pushed to one side. Even a small difference in impedance of the channels on one side compared to the other will cause the jet to shift from the center line. Thus the possibility of good quality data having a reduced flow rate due to clogging is extremely low.

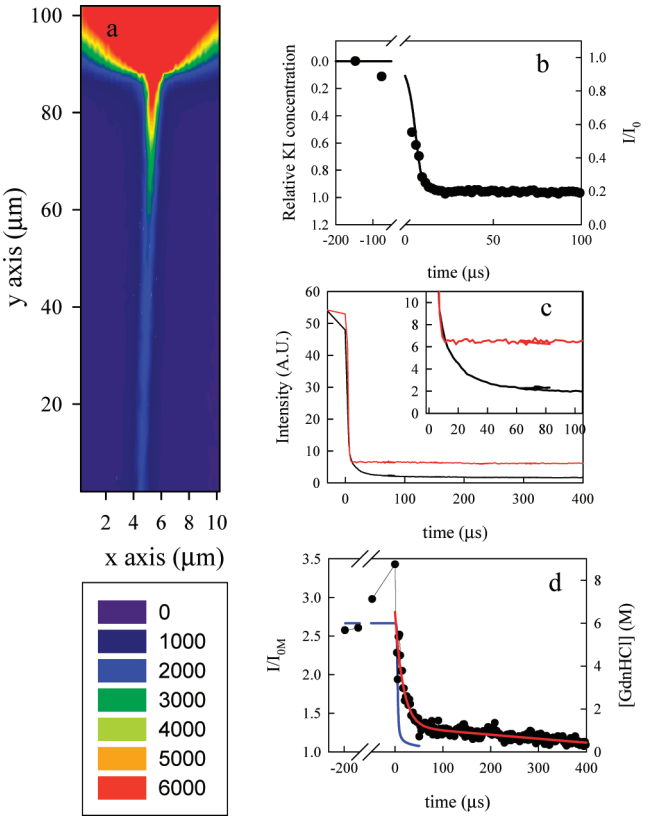

Figure 1. Observation of Trp fluorescence in the microfluidic mixer. (a) Contour plot of intensity near the mixing region. The denatured protein (in 6 M GdnHCl) enters from the top and is constricted to a narrow jet by side channel flows at ~90 μm on the y-axis. The protein then continues down the exit channel as it folds. (b) Concentration along the center streamline of the exit channel of 400 mM KI, a fluorescence quencher of N-acytltryptophan amide (NATA). The line is the concentration calculated by COMSOL (left axis) and the points are the measured ratio of intensities of NATA fluorescence with and without KI (right axis). Time is calculated based on an increasing velocity within the mixing region. (c) Total intensity of villin within 1 μm around the jet as a function of time. The black line is the kinetics after mixing into 0 M GdnHCl from 6 M GdnHCl and the red line is the kinetics after mixing into 6 M GdnHCl. The rapid drop at $t = 0$ is due to the formation of the jet. (Inset) Close up of trajectories during and after mixing. (d) Relative intensity (compared to a folded sample in 0 M GdnHCl) of villin mixed into 0 M GdnHCl (black points and line). The red line is a fit to the data for the function $y = a + b\exp(-kt) - ct$. The blue line (right axis) is the calculated concentration of GdnHCl in the mixing region.

Fluorescence changes can be observed at various times beyond mixing using the same confocal instrument described by Lapidus et al.[28] Briefly, the Trp is excited with a doubled argon-ion laser at 258 nm (Lexel Laser 95 SHG, Fremont, CA) focused by an infinity-corrected 0.5 NA objective (OFR 40x-266, Newton, NJ) and the resulting fluorescence captured by the same objective and detected by a photon counting module. Scattered laser light is removed by a 300 nm dichroic mirror (Chroma 300dclp, Brattleboro, VT), a UG1 filter and a 100 μm pinhole placed at the focus of the detected light in front of the detector (Hamamatsu H7421−40, Hamamatsu City, Japan). The chip is scanned over the objective by a piezoelectric scanner (Mad City Laboratories Nano-LP100, Madison, WI) for fine resolution and by a motorized microscope stage (Semprex KL46, Campbell, CA) for coarse resolution. The temperature of the mixing chip and all solutions is raised or lowered by an aluminum manifold in contact with two thermoelectric devices (TE Technology CH-77-1.0-0.8, Traverse City, MI) and controlled to within 0.005 °C by a temperature controller (TE Technology model 1600).

To ensure that the data after mixing is not affected by the mixer response, measurements are made using two different flow rates on the same chip and same day (typically 0.5 and 1.0 m/s). After converting the distance from the mixing region to time, the data in the mixing region for the slow flow rate (~0−30 μs) is deleted to remove the slower mixer response. All remaining data must overlap the signal response at the faster flow rate or the entire data set is discarded.

The T-jump instrument is identical to that used in refs 20 and 21. The peptide was dissolved to 100 μM in 20 mM acetate buffer at pH 4.9. Equilibrium fluorescence was measured on a Photon Technology International fluorimeter. The protein concentration was 20 μM

RESULTS AND DISCUSSION

For the measurements presented in this work, we use the N27H mutant of the villin headpiece subdomain HP-35. At low pH the presence of a protonated histidine four residues away from the sole tryptophan induces a decrease in fluorescence quantum yield when the C-terminal helix is formed.[21] Typically the protein is dissolved in 6 M GdnHCl and placed in the center channel of a microfabricated mixer. In the mixing region, this channel is rapidly mixed with buffer from two side channels that flow 100 times faster. The relatively large and therefore more slowly diffusing protein molecules are constricted to a jet ~100 nm wide (see Figure 1a) while the smaller denaturant molecules are diffusively mixed within a few micrometers. Figure 1b illustrates the mixing profile; the plot shows the computed change in concentration of potassium iodide (KI), a fluorescence quencher, as a function of distance along with a measurement of relative loss of fluorescence due to mixing *N*-actyltryptophan amide with KI. The mixing time, the time for the concentration to change by 80%, is ~8 μs. Beyond 8 μs, there is a slight exponential decay in the concentration, but the amplitude of this decay is very small (10% of the total change) and slightly faster than the observed folding decay (compare the blue and red lines in Figure 1d). This implies that any decay after this time is due entirely to folding. Beyond the mixing region the protein jet flows at a constant rate down the 500 μm exit channel and Trp fluorescence is observed at various points along this channel with a confocal microscope with 1 μm resolution. Figure 1c shows the Trp intensity as a function of time. Near $t = 0$ there is a large drop in intensity due to formation of the jet

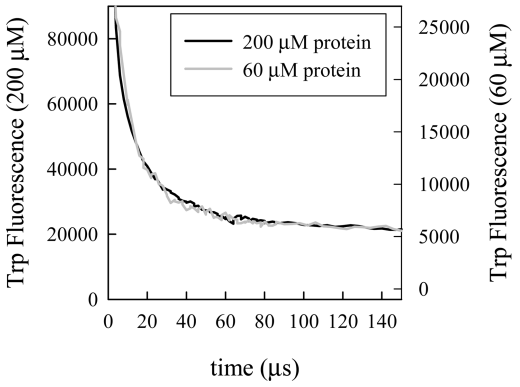

Figure 2. Relaxation kinetics of villin after dilution of denaturant for two different concentrations of protein: 200 μM (black line, left axis) and 60 μM (gray line, right axis).

and then further exponential decay due to folding (black line). A control experiment, in which the denaturant is not diluted from 6 M GdnHCl (red line) shows the same decrease in intensity near $t = 0$ as the experiment in which the denaturant is diluted to ~0 M GdnHCl, indicating there is little or no "burst phase" or loss of fluorescence within the first 10 microseconds. Another way to examine the burst phase is to compare the folding trajectory point-by-point with another trajectory of the folded protein in 0 M GdnHCl to remove mixing and optical effects (see Figure 1d). A fit to the data after 12 μs of a single exponential plus a linear decay in Figure 1d shows that the extrapolation of the fit to $t = 0$ agrees well with the relative amplitude prior to mixing. Measurements at different concentrations of protein show no change in the kinetic decay, indicating that the measurement is not affected by aggregation (see Figure 2).

The data after mixing does not fit well to a single exponential but requires another phase. This phase could be an optical or flow effect not removed by normalization, but it is quite reproducible across different experiments on different chips. Therefore we cannot rule out this slow decay is yet another folding process. Two exponentials fit the data, but because the slower phase is so small and so slow, we find more consistent results to use an exponential plus a linear function. Only the exponential rates will be considered quantitatively here.

The exponential rates from mixing are plotted in Figure 3, panels a and b. Also plotted in Figure 3a are T-jump measurements completed on exactly the same peptide sample used in the mixer experiments. The rates from T-jump are very similar to those measured previously on the uncapped sequence by Kubelka et al. The lines on Figure 3, panels a and b, show the folding and unfolding rates extracted from T-jump experiments using a two-state model.[20,21] The equilibrium amplitudes of the decays are plotted in Figure 3, panels c and d, and show good qualitative agreement with equilibrium measurements.[20,21] Unfolding experiments in which the folded protein in 0 M GdnHCl is mixed into various high concentrations of GdnHCl show overlap with the folding rates near the midpoint, 2.5 M GdnHCl, but diverge from the folding rates at 3−4 M GdnHCl. An Arrhenius fit ($k \propto \exp(-m^*[\mathrm{GdnHCl}]/RT)$) to all folding rates (black points) at [GdnHCl] <3 M (Figure 1b) gives an *m*-value of 0.16 kcal/mol/M.

Based on the rate and amplitude data in Figure 3, it appears that, after dilution of denaturant, HP-35 folds in a single step and reaches equilibrium within 0.5 ms. There is no evidence of any type of intermediate, misfolded state or aggregation. If the

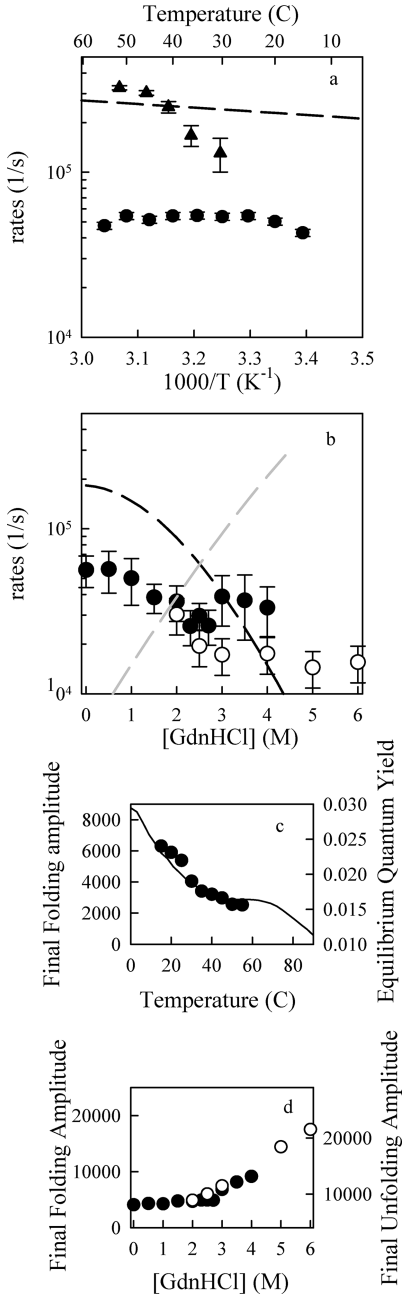

Figure 3. Relaxation rates of HP-35 after dilution of denaturant at various temperatures (a) and [GdnHCl] (b). The black circles started from an initial [GdnHCl] = 6 M, and the white circles in panel b started from an initial [GdnHCl] = 0 M. The final denaturant concentration in panel a is [GdnHCl]~0.1 M. The error bars represent the reproducibility of fitted rates from different experiments on different days with different mixing chips. The triangles are relaxation rates measured by T-jump. The dashed lines in panels a and b are the fitted folding (black) and unfolding (gray) rates from T-jump data and are taken from refs 20 and 21. Final amplitudes of the relaxations for the rates in panels a and b are shown in panels c and d, respectively (circles). The line in panel c is the fluorescence quantum yield measured in equilibrium (right axis).

T-jump and mixing experiments were sampling distinct alternate pathways we might expect either method to show biexponential kinetics, but T-jump kinetics clearly reach equilibrium within 10 μs and mixer kinetics show no burst phase amplitude before 10 μs (see inset to Figure 1, panels b and d). This is, to our knowledge, one of the first observations of kinetics that depend on starting conditions. Liu et al observed a small decrease in relaxation rates of the Fib35 WW domain for T-jumps of 5−7 C compared to jumps of 10−11 C, but the difference in rates is less than a factor of 2 and within the scatter in the data.[29]

How then do we reconcile this apparent simple two-state behavior with relaxation rates measured by T-jump that are 4−5 times faster? One possibility is that there is no energetic barrier to folding. Such a landscape may show probe-dependent kinetics such as observed for lambda-repressor.[5,6] However, Cellmer et al.[30] showed that the folding rates for villin obtained by T-jump with monitoring by Trp fluorescence and loop closure in the unfolded state[31] yield identical folding rates in a two-state analysis where the initial as well as the final conditions are very similar. Furthermore, other work suggests villin is not perfectly two-state.[30] Kubelka et al. observed an extremely fast phase attributed to helix fraying.[21] Reiner et al., also measuring loop closure in equilibrium, have found a near-native "unlocked" state which interconverts with the locked state in ~1 μs. These states are likely indistinguishable by our measurements as helix 3, where the Trp is located, is formed in both states. Reiner et al. also identified a high energy intermediate on the native-side of the major energy barrier that would not be rate-limiting for folding or unfolding experiments.[32] Thus sequential low free energy barriers may not account for the results in this work. Perhaps for villin, after rapid T-jump and rapid mixing, the unfolded ensembles are not the same and therefore relax on the final landscape in different ways.

In order to quantitatively interpret the kinetics of both T-jump and mixing experiments, we turn to the slightly more complex "Thruway Search Model",[33] in which the unfolded macrostate of m microstates can be divided into two subsets, a set of unfolded conformations, D_o, with direct access to the native state, N, and a set that are dead-ends or kinetic traps, D_m. Assuming a single barrier between D_o and N and the number of routes to the native state, n, and the intrachain interaction energy of unfolded states, e, Ghosh et al. fit the T-jump kinetic data for HP-35 using $\log(n) = 16.94$, $e = 0.62$ kcal/mol and microscopic barrier heights $\varepsilon_{DN} = 24.0\ kT$ and $\varepsilon_{ND} = 47.6\ kT$[33] [the macroscopic free energy barrier is $\Delta G^{\ddagger}(T) = \varepsilon_{DN} - kT \ln(n/m(T))$]. Using the same barrier height, we can fit the mixing kinetic rates by increasing $\log(n) = 18.54$ and decreasing $e = 0.49$ kcal/mol (see Figure 4a). Figure 4b shows that the number of unfolded states in the fit to the mixing data is significantly higher than the number of unfolded states (m) in the fit to the T-jump data and this difference increases with temperature. The number of states, m, depends on the unfolded state density ρ as $m = \exp[-L((1-\rho)/\rho)\ln(1-\rho)]$ where L is the number of amino acids in the chain. This shows the increase in m is related to the decrease in ρ implying a high value of m is associated with a bigger radius of gyration on average.[33] Thus this model shows that the average unfolded conformation after dilution of denaturant is more expanded than the average unfolded conformation at high temperature, a conclusion that is in broad agreement with recent single-molecule studies of unfolded proteins.[34,35] Previous mixing studies have shown that denatured proteins collapse on the submicrosecond time-scale,[28] but it is quite possible that the unfolded state reached after dilution of denaturant is still more expanded than that reached by increasing the temperature to unfold the protein.

If one describes the folding energy landscape as one-dimensional, one can imagine that the relaxation after a large change in shape of the landscape (such as for mixing) might be quite distinct from

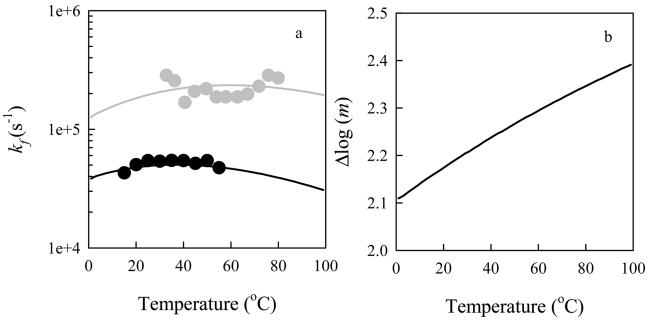

Figure 4. (a) Measured folding rates of HP-35 by T-jump (gray points) and dilution of denaturant (black points) vs temperature. The lines are rates calculated by the Thruway Search Model described in the text with the parameters in the text. (b) Ratio of the total number of unfolded states of the mixing experiment to T-jump vs temperature.

relaxation after a small change (such as for T-jump). Recently a coarse-grained model described a two-dimensional landscape based on the two halves of the villin chain found asymmetry in the landscape in which the first two helices form more easily than the last helix at low temperature, but this asymmetry disappears at high temperature.[36] If the high temperature landscape resembles high denaturant, then rapid mixing would produce unfolded conformations far from the asymmetric minimum, perhaps leading to slower folding.

Figure 3b shows that the unfolding rates measured by mixing (white points) are also significantly lower than that measured by T-jump. It is possible that this difference can also be attributed to differences in the starting conditions for these two measurements (0 M GdnHCl, 23 C for mixing, high denaturant and ~30 C for T-jump). However, the Thruway Search Model assumes that the folded protein has a single or small ensemble of native states that do not change with starting conditions and therefore cannot account for this difference. The model can explain the folding data and the differences between the T-jump and mixing experiments and also extract certain features of the folding landscape such as the number of paths, size of the denatured ensemble, and barrier height. However, it does not provide a first principle approach to predict such parameters. In order to explain starting condition dependent kinetics, as observed here, and predict the parameters of the complex landscape, one needs a more microscopic treatment.

There have been numerous molecular dynamics simulations of this protein with varying complexity from simple bead models up to full atom simulations in explicit solvent. Each has examined different aspects of folding but has noted details that add complexity to the folding path. For example, Lei et al., using implicit solvent simulations, have identified an on-pathway and an off-pathway intermediate.[16] Using explicit solvent, Freddolino et al. found that, if the protein forms all three helices very early, it then spends a long time exploring non-native conformations before dissociating and locking into the native state and identified a specific long-lived misfolded state in which helix 1 is flipped the wrong way relative to helix 2 and 3.[13] More recently, Lei et al has constructed a folding network with multiple pathways visited by five separate simulations.[37] Simulators typically have a fairly small number of trajectories to analyze, but a study by Ensign et al. looked at over 100 trajectories that reached at least 1 μs of a fast folding mutant which folds in about 800 ns. This study detected a significant fraction of trajectories that did not fold within the 1−2 μs simulation time.[17] Later work by Bowman et al. created a Markov state model of this mutant and showed that the folding times were exponentially distributed near the measured rate from T-jump but longer rates were possible. Additionally, the model revealed that the mean-first-passage times between unfolded states were more than 100 times longer than the folding rates such that the protein is more likely to fold than to reconfigure to another unfolded conformation.[10] In this sort of scenario, it is easy to imagine that some unfolded states, especially those with highly expanded conformations, progress significantly more slowly to the folded state than the average pathway. In light of the results presented here, future work should examine how the observed folding pathways depend on how likely a starting conformation is populated in a real ensemble. More generally, computational exploration of an energy landscape must also consider how that landscape is populated in a real experiment or within a cell.

■ ACKNOWLEDGMENT

We thank William Eaton, Ken Dill, and Vijay Pande for many helpful discussions. This work is supported by National Science Foundation FIBR (NSF EF-0623664). This work was partially supported by funding from National Science Foundation FIBR Grant 0623664 administered by the Center for Biophotonics, an NSF Science and Technology Center, managed by the University of California, Davis, under Cooperative Agreement PHY 0120999. The research of L.L., Ph.D. is supported in part by a Career Award at the Scientific Interface from the Burroughs Welcome Fund.

■ REFERENCES

(1) Scalley, M. L.; Yi, Q.; Gu, H. D.; McCormack, A.; Yates, J. R.; Baker, D. *Biochemistry* **1997**, *36*, 3373–3382.
(2) Segel, D. J.; Bachmann, A.; Hofrichter, J.; Hodgson, K. O.; Doniach, S.; Kiefhaber, T. *J. Mol. Biol.* **1999**, *288*, 489–499.
(3) Bryngelson, J. D.; Onuchic, J. N.; Socci, N. D.; Wolynes, P. G. *Proteins-Struct., Funct., Genet.* **1995**, *21*, 167–195.
(4) Dill, K. A.; Chan, H. S. *Nat. Struct. Biol.* **1997**, *4*, 10–19.
(5) Ma, H. R.; Gruebele, M. *Proc. Natl. Acad. Sci. U.S.A.* **2005**, *102*, 2283–2287.
(6) DeCamp, S. J.; Naganathan, A. N.; Waldauer, S. A.; Bakajin, O.; Lapidus, L. J. *Biophys. J.* **2009**, *97*, 1772–1777.
(7) Hagen, S. J. *Proteins-Struct., Funct., Bioinformat.* **2007**, *68*, 205–217.
(8) Rajan, A.; Freddolino, P. L.; Schulten, K. *Plos One* **2010**, 5.
(9) Lee, I. H.; Kim, S. Y.; Lee, J. *J. Comput. Chem.* **2010**, *31*, 57–65.
(10) Bowman, G. R.; Pande, V. S. *Proc. Natl. Acad. Sci. U.S.A.* **2010**, *107*, 10890–10895.
(11) Xiao, S. F.; Bi, Y.; Shan, B.; Ralelgh, D. P. *Biochemistry* **2009**, *48*, 4607–4616.
(12) Meng, W. L.; Shan, B.; Tang, Y. F.; Raleigh, D. P. *Protein Sci.* **2009**, *18*, 1692–1701.
(13) Freddolino, P. L.; Schulten, K. *Biophys. J.* **2009**, *97*, 2338–2347.
(14) Bagchi, S.; Falvo, C.; Mukamel, S.; Hochstrasser, R. M. *J. Phys. Chem. B* **2009**, *113*, 11260–11273.
(15) Sonavane, U. B.; Ramadugu, S. K.; Joshi, R. R. *J. Biomol. Struct. Dyn.* **2008**, *26*, 203–214.
(16) Lei, H. X.; Duan, Y. *J. Mol. Biol.* **2007**, *370*, 196–206.
(17) Ensign, D. L.; Kasson, P. M.; Pande, V. S. *J. Mol. Biol.* **2007**, *374*, 806–816.
(18) Mukherjee, A.; Bagchi, B. *J. Chem. Phys.* **2004**, *120*, 1602–1612.
(19) Duan, Y.; Kollman, P. A. *Science* **1998**, *282*, 740–744.
(20) Cellmer, T.; Henry, E. R.; Kubelka, J.; Hofrichter, J.; Eaton, W. A. *J. Am. Chem. Soc.* **2007**, *129*, 14564–+.

(21) Kubelka, J.; Eaton, W. A.; Hofrichter, J. *J. Mol. Biol.* **2003**, *329*, 625–630.
(22) Brewer, S. H.; Song, B. B.; Raleigh, D. P.; Dyer, R. B. *Biochemistry* **2007**, *46*, 3279–3285.
(23) Kubelka, J.; Henry, E. R.; Cellmer, T.; Hofrichter, J.; Eaton, W. A. *Proc. Natl. Acad. Sci. U.S.A.* **2008**, *105*, 18655–18662.
(24) Knight, J. B.; Vishwanath, A.; Brody, J. P.; Austin, R. H. *Phys. Rev. Lett.* **1998**, *80*, 3863–3866.
(25) Hertzog, D. E.; Ivorra, B.; Mohammadi, B.; Bakajin, O.; Santiago, J. G. *Anal. Chem.* **2006**, *78*, 4299–4306.
(26) Hertzog, D. E.; Michalet, X.; Jager, M.; Kong, X. X.; Santiago, J. G.; Weiss, S.; Bakajin, O. *Anal. Chem.* **2004**, *76*, 7169–7178.
(27) Yao, S.; Bakajin, O. *Anal. Chem.* **2007**, *79*, 5753–5759.
(28) Lapidus, L. J.; Yao, S.; McGarrity, K. S.; Hertzog, D. E.; Tubman, E.; Bakajin, O. *Biophys. J.* **2007**, *93*, 218–224.
(29) Liu, F.; Dumont, C.; Zhu, Y. J.; DeGrado, W. F.; Gai, F.; Gruebele, M. *J. Chem. Phys.* **2009**, 130.
(30) Cellmer, T.; Buscaglia, M.; Henry, E. R.; Hofrichter, J.; Eaton, W. A. *Proc. Natl. Acad. Sci.* **2011**, *108*, 6103–6108.
(31) Lapidus, L. J.; Eaton, W. A.; Hofrichter, J. *Proc. Natl. Acad. Sci. U.S.A.* **2000**, *97*, 7220–7225.
(32) Reiner, A.; Henklein, P.; Kiefhaber, T. *Proc. Natl. Acad. Sci.* **2010**.
(33) Ghosh, K.; Ozkan, S. B.; Dill, K. A. *J. Am. Chem. Soc.* **2007**, *129*, 11920–11927.
(34) Merchant, K. A.; Best, R. B.; Louis, J. M.; Gopich, I. V.; Eaton, W. A. *Proc. Natl. Acad. Sci. U.S.A.* **2007**, *104*, 1528–1533.
(35) Sherman, E.; Haran, G. *Proc. Natl. Acad. Sci. U.S.A.* **2006**, *103*, 11539–11543.
(36) Wolff, K.; et al. *EPL* **2011**, *94*, 48005.
(37) Lei, H.; Chen, C.; Xiao, Y.; Duan, Y. *J. Chem. Phys.* **2011**, *134*, 205104–205107.